Available online at www.sciencedirect.com
ScienceDirect
Trans. Nonferrous Met. Soc. China 31(2021) 1969−1978
Transactions of Nonferrous Metals Society of China
www.tnmsc.cn

Microstructure and mechanical properties of high strength Mg−15Gd−1Zn−0.4Zr alloy additive-manufactured by selective laser melting process

Peng-huai FU[1,2], Nan-qing WANG[1], Hai-guang LIAO[1], Wen-yu XU[1], Li-ming PENG[1], Juan CHEN[1], Guo-qi HU[3], Wen-jiang DING[1]

1. National Engineering Research Center of Light Alloy Net Forming and State Key Laboratory of Metal Matrix Composite, Shanghai Jiao Tong University, Shanghai 200240, China;
2. Shanghai Light Alloy Net Forming National Engineering Research Center Co., Ltd., Shanghai 201615, China;
3. School of Materials and Chemical Engineering, Ningbo University of Technology, Ningbo 315211, China

Received 5 July 2020; accepted 19 January 2021

Abstract: In order to verify the feasibility of producing Mg−rare earth (RE) alloy by selective laser melting (SLM) process, the microstructure and mechanical properties of Mg−15Gd−1Zn−0.4Zr (wt.%) (GZ151K) alloy were investigated. The results show that fine grains (~2 μm), fine secondary phases and weak texture, were observed in the as-fabricated (SLMed) GZ151K Mg alloy. At room temperature, the SLMed GZ151K alloy has a yield strength (YS) of 345 MPa, ultimate tensile strength (UTS) of 368 MPa and elongation of 3.0%. After subsequent aging (200 °C, 64 h, T5 treatment), the YS, UTS and elongation of the SLMed-T5 alloy are 410 MPa, 428 MPa and 3.4%, respectively, which are higher than those of the conventional cast-T6 alloy, especially with the YS increased by 122 MPa. The main strengthening mechanisms of the SLMed GZ151K alloy are fine grains, fine secondary phases and residual stress, while after T5 treatment, the YS of the alloy is further enhanced by precipitates.
Key words: selective laser melting; Mg−rare earth alloy; grain refinement; Mg−Gd−Zn; strengthening mechanism

1 Introduction

As one of the lightest structural materials, magnesium−rare earth (Mg−RE) alloys with high specific strength and low density are the most promising materials for lightweight applications, such as in automobile, aerospace and medical industries [1−3]. Up to now, all of high strength casting magnesium alloys are Mg−RE alloys, such as Mg−Y−Nd (WE series) [4,5], Mg−Gd−Y [6,7], Mg−Gd(Y)−Zn [8−11], and Mg−Gd(Y)−Ag [12−14] based alloys. At present, the majority of Mg–RE parts are manufactured by permanent mold and sand mold casting [11,15,16], and frequently suffer from the problems of casting defects, limited part accuracy, relatively poor mechanical properties and very long developing cycles, which limit their actual applications. Therefore, new manufacturing technologies are needed to produce high quality Mg−RE alloy parts.

Selective laser melting (SLM), as an emerging manufacturing technique for metal components, is used to build parts by selectively melting metal powders layer by layer. With its advantages of high dimensional precision, ability to build complex geometries and mouldless manufacturing, SLM process has been successfully applied to traditional structural metal materials including steel, titanium alloy, and aluminum alloy, which exhibit comparable mechanical performances with their counterparts made by casting or even forging. In

Corresponding author: Peng-huai FU, Tel: +86-21-34202794, E-mail: fph112sjtu@sjtu.edu.cn
DOI: 10.1016/S1003-6326(21)65630-3

terms of Mg alloys, only limited studies were conducted on Mg−Al [17,18], Mg−Zn [19,20] and WE43 (Mg−Y−Nd based) [21−23] alloys. The as-fabricated WE43 alloy [22] indicated very fine grains ranging from 0.4 to 2.9 μm with a mean grain size of 1.0−1.1 μm, and excellent tensile properties at room temperature: yield strength (YS) of ~300 MPa, ultimate tensile strength (UTS) of 308 MPa and elongation of 12.2%. It seems that the very high cooling rate of SLM process in an order of 10^6 K/s [24] leads to fine microstructure, which enhances the tensile performance. Very fine grains of 1.0−2.9 μm were also reported in the SLMed AZ91D alloy [17], which are much finer than those of permanent mold cast AZ91D alloy (average grain size of ~119 μm [25]). Therefore, SLM process could be used to produce fine-grained Mg components, where fine grains are good for both strength and ductility. In order to verify the feasibility of producing Mg−rare earth (RE) alloy by SLM process, Mg−15Gd−1Zn−0.4Zr (wt.%) (GZ151K) Mg−RE alloy [10], one of the strongest casting Mg alloys, was fabricated. Microstructure and mechanical properties of the SLMed GZ151K alloy and the influence of subsequent aging treatment (T5, without solution treatment) were studied and compared with those of its permanent mold cast counterpart [10].

2 Experimental

Centrifugal-atomized spherical powders of Mg−15Gd−1Zn−0.4Zr (GZ151K, wt.%) alloy (Tangshan Weihao Magnesium Powder Co., Ltd., China) and a commercial ZRapid SLM 150 machine with IPG fiber laser of 200 W (ZRapid Tech Co., Ltd., China) were used. Powder bed and Mg–RE substrate were pre-heated at 100 °C for 30 min before printing. During SLM process, working chamber was full of argon and the oxygen content was controlled below 0.05 vol.%. The following optimized process parameters were used: laser power of 200 W, scanning speed of 700 mm/s, layer thickness of 30 μm, hatch spacing of 70 μm, and scanning direction rotated by 73° between neighboring layers. Similar to laser melting deposition (LMD) process [26], during the SLM process of GZ151K alloy, serious spattering appeared, as shown in Fig. 1(a). The spattering was much more obvious in GZ151K alloy than that in steel, Ti or Al alloys. Square blocks of 8 mm × 8 mm × 5 mm (5 mm is the thickness along the building direction or z direction in Fig. 1(b)) were built for the microstructure observation and bone-shaped samples with gauge dimensions of 18 mm × 3 mm × 10 mm (10 mm is the thickness in building direction) were built for tensile tests. The bone-shaped samples were cut into pieces and tensile samples with 3 mm in width and 1.5 mm in thickness in the gauge section were got. The tensile samples were tested on a Zwick Z100 test machine under 0.5×10^{-3} s^{-1} at room temperature, and tensile direction was perpendicular to the building direction and along the y direction in Fig. 1(b). Since layer cracks perpendicular to the building direction in bone-shaped samples were frequently observed (indicated by arrows in Fig. 1(b)), the mechanical properties fluctuated greatly and only the best tensile properties of as-fabricated (SLMed) and T5 treated (200 °C, 64 h, SLMed-T5) alloys were selected. The detailed manufacturing process of cast GZ151K alloy can be seen in Ref. [10]. The cast ingots were heated to 500 °C and kept for 2 h followed by the solution treatment at 520 °C for 12 h, and then quenched into ~90 °C water. The

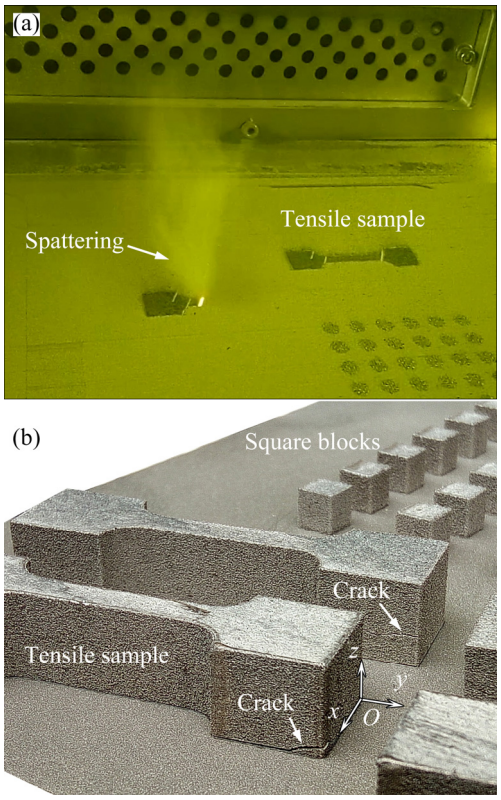

Fig. 1 Spattering of GZ151K alloy powders during SLM process (a) and SLMed samples of GZ151K alloy (b)

solution-treated specimens were then aged at 200 °C for 64 h in an oil bath (Cast-T6).

The density of square blocks was measured via Archimedes method and the average density is 1.929 g/cm^3. The theoretical density of GZ151K alloy is 1.971 g/cm^3, which means the relative density of the SLMed GZ151K alloy is 97.9%. The chemical compositions of the powders and the SLMed alloy were identified by ionized coupled plasma (ICP) and are listed in Table 1. It could be found that the contents of Gd, Zn and Zr in SLMed alloy are higher than those in the powders, respectively. Similar results were also reported in SLMed WE43 alloy [22], which was attributed to the evaporation of Mg during the SLM process. Microstructure (*xz* plane in Fig. 1(b)) of the SLMed alloy was observed in a Zeiss Axio Observer A1 optical microscope (OM) and a NOVA Nano 230 SEM with an energy dispersive spectrometer (EDS). Electron backscattered diffractometer (EBSD) was used to obtain the texture information. The EBSD raw data were processed in commercial software of TSL OIM 8.5. Phases were identified by an Ultima IV X-ray diffraction (XRD) spectrometer with a scanning speed of 5 (°)/min. The fracture surfaces were also observed in an SEM.

Table 1 Chemical compositions of centrifugal-atomized GZ151K powders and SLMed GZ151K alloy (wt.%)

Material	Gd	Zn	Zr	Mg
Powder	13.57	0.85	0.30	Bal.
SLMed alloy	13.86	0.95	0.31	Bal.

3 Results

3.1 Microstructure

Figure 2 shows SEM images of the GZ151K powders and their cross-section. It shows that most of the powders are globularly shaped, some of which are sticked to small balls or irregular particles. Generally, the diameters of the powders change from 25 to 65 μm, with the average of about 47 μm. From the cross-section image, it could be found that the powders have very fine grains of ~2.5 μm on average, and finer powders have finer grains.

Figure 3 shows OM and SEM images of the SLMed and permanent mold cast GZ151K alloys.

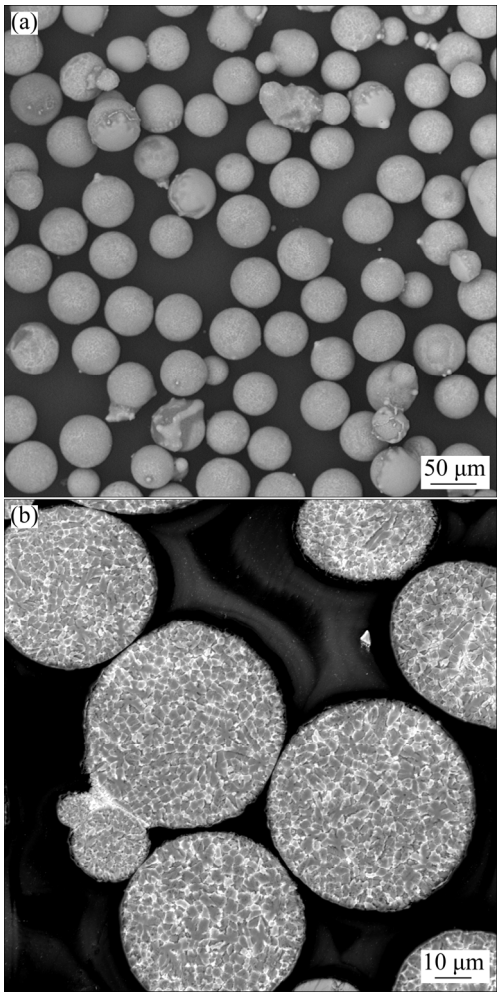

Fig. 2 SEM images of GZ151K powders (a) and their cross-section (b)

In OM image (Fig. 3(a)), fish-scale-shaped melt pools are clearly revealed. The boundaries of melt pools are visible because the microstructures beside the boundaries are different, as shown in Fig. 3(b). The boundary is roughly represented by the dotted lines. Compared with the microstructures on the left side of the boundary, the secondary phases and grains on the right side of the boundary are larger, specially the secondary phases. The larger secondary phases and coarser grains on the right side should be formed due to the heat influence of the left side. During the SLM process, the right side solidifies firstly, and then the left side. The released heat during the solidification of the left side makes the secondary phases and grains on the right side grow larger. Similar microstructures were also observed in SLMed AZ91D [17] and ZK60 [19] Mg alloys. Figure 3(c) shows SEM image of permanent mold cast GZ151K alloy. Compared with those of

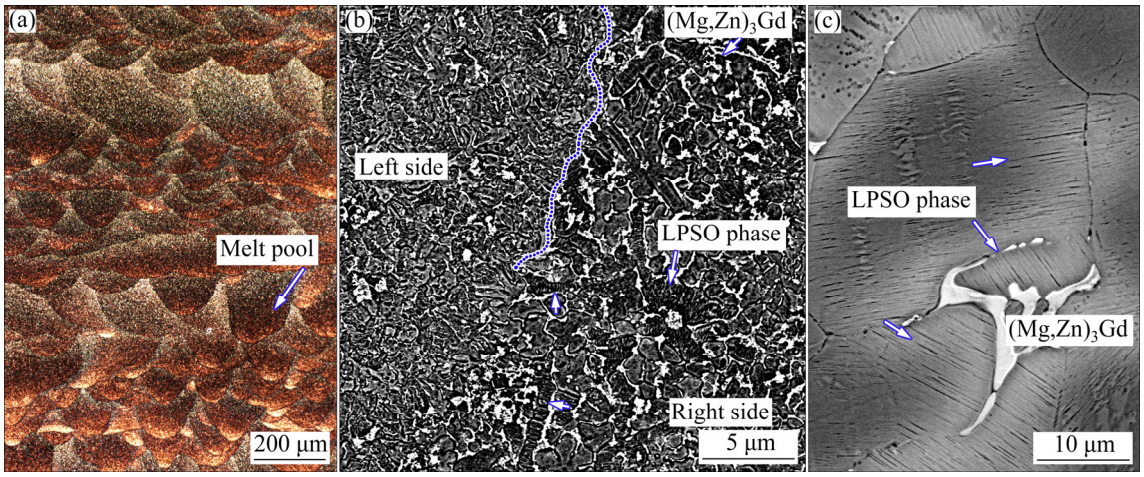

Fig. 3 OM (a) and SEM (b) images of SLMed GZ151K alloy from side view of *xz* plane in Fig. 1(b), and SEM image of permanent mold cast GZ151K alloy (c)

the SLMed alloy, the grains and secondary phases of the cast GZ151K alloy are much larger. According to the previous study [10], the large secondary phases along the grain boundary are $(Mg,Zn)_3Gd$ phase and fine lamellar phases at grain interiors (indicated by arrows in Fig. 3(c)) are 14H-type LPSO (long period stacking ordered) phases [27,28]. Very fine lamellar phases can also be observed in the SLMed GZ151K alloy, as indicated by the arrows in Fig. 3(b).

Figure 4 shows the XRD patterns of the GZ151K powders and the SLMed GZ151K alloy. They both consist of α-Mg matrix, Mg_3Gd and GdH_2 phases. For Mg_3Gd phase, the intensity of the XRD peaks decreases from the powders to the SLMed alloy, which probably indicates that the content of Mg_3Gd phase decreases after SLM process. While the intensity of GdH_2 phase increases, probably indicating that there is a rise in the content of GdH_2 during the SLM process. Unfortunately, at the current image resolution (Figs. 2(b) and 3(b)), it is hard to distinguish the two phases. From the previous study [29], it could be found that REH_2 phases were usually very fine in as-cast conditions, and they grew up during high temperature solution. Therefore, in the SLMed GZ151K alloy, GdH_2 phases are probably very fine and most of the compounds observed in Figs. 2(b) and 3(b) should be Mg_3Gd compounds.

Figure 5 shows the EBSD mapping images of the SLMed GZ151K alloy from the side and top views. Microstructures in both views consist of fine equiaxed-grains, while the grain size in the top view

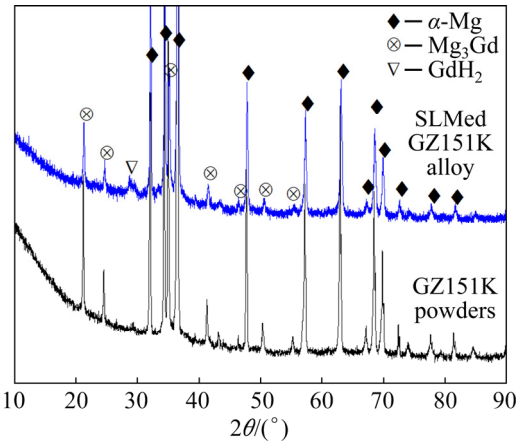

Fig. 4 XRD patterns of centrifugal-atomized GZ151K powders and SLMed GZ151K alloy

is a little bit finer than that in the side view. The average grain size of the SLMed alloy is approximately 2 μm, which is much finer than that of the cast GZ151K alloy (41 μm) [10]. The SLMed alloy shows weak textures, and the maximum intensities of texture from side and top views are 3.07 and 2.35, respectively.

Figure 6 shows TEM bright field images of the T5-treated SLMed (SLMed-T5) GZ151K alloy aged at 200 °C for 64 h. It could be found from Fig. 6(a) that, there are larger compounds along the grain boundaries. As the analysis above, these large compounds are probably Mg_3Gd phases, and they are very stable during aging process. Besides the large Mg_3Gd phases, very fine particles, as shown in the inserted image in Fig. 6(a), are also observed at grain interiors. EDS results indicate that these

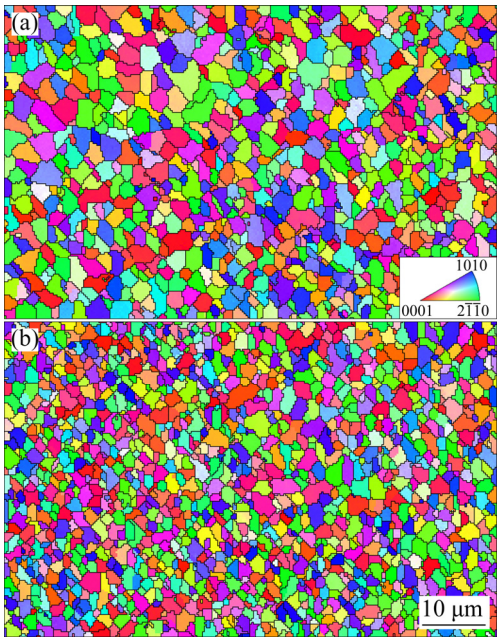

Fig. 5 EBSD mapping images of SLMed GZ151K alloy: (a) Side view of *xz* plane in Fig. 1(b); (b) Top view of *xy* plane in Fig. 1(b)

particles contain 54−67 wt.% Gd, which agrees well with the Gd content (68 wt.%) in Mg_3Gd phase. Therefore, these fine particles are probably Mg_3Gd phases and they precipitate and grow up during the SLM process.

Besides these equilibrium Mg_3Gd phases along the grain boundaries and at grain interiors, two kinds of metastable precipitates, long basal precipitates and prismatic precipitates, are also observed, as shown in Figs. 6(b, c). The long basal precipitates have very large aspect ratio and there are un-continuous streaks along $[0001]_\alpha$ in the SAED pattern (indicated by the inserted image in Fig. 6(b)), both of which are consistent well with the characteristics of the basal γ' precipitates observed in the Mg−1Gd−0.4Zn−0.2Zr (at.%) alloy [30]. Therefore, the long basal precipitates here could be identified as γ' precipitates, which have a disordered hexagonal structure (space group $P\bar{3}m1$, a=0.321 nm and c=0.780 nm) and a MgGdZn composition [30]. The basal γ' precipitates were also found in cast-T6 GZ151K alloy [10] and cast-T6 Mg−12Gd−0.8Zn−Zr (wt.%) alloy [11,31]. The morphologies of the prismatic precipitates are not very clear, but with clear lattice fringes, as indicated by the arrows in Fig. 6(c). From the extra diffraction spots in the SAED pattern in Fig. 6(b), indicated by the smaller arrows, it could be found that these precipitates are the β' meta-stable phases with cbco structure, which are frequently observed in Mg−Gd based alloys [1−3]. Compared with the cast-T6 GZ151K [10] and Mg−12Gd−0.8Zn−Zr [11] alloys, the number densities of both β' and γ' precipitates are much lower here. It is probably due to lower content of solution elements in the matrix of the SLMed GZ151K alloy, and most of alloy elements form Mg_3Gd phases along the grain boundaries and at grain interiors (Fig. 6(a)).

3.2 Mechanical properties

Figure 7 shows the engineering stress−strain curves and tensile properties of the SLMed and SLMed-T5 GZ151K alloys at ambient temperature.

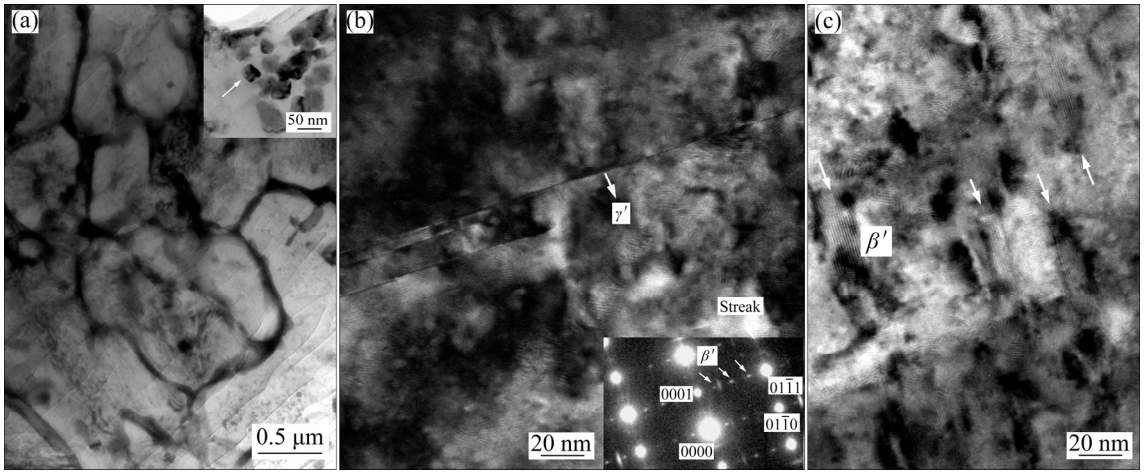

Fig. 6 TEM bright field images of SLMed-T5 GZ151K alloy: (a) Overall morphology indicating secondary phases along grain boundaries with inserted image illustrating secondary phases at grain interiors; (b) Basel γ' precipitates at grain interiors observed from $[2\bar{1}\bar{1}0]_\alpha$; (c) Prismatic β' precipitates at grain interiors observed from $[2\bar{1}\bar{1}0]_\alpha$

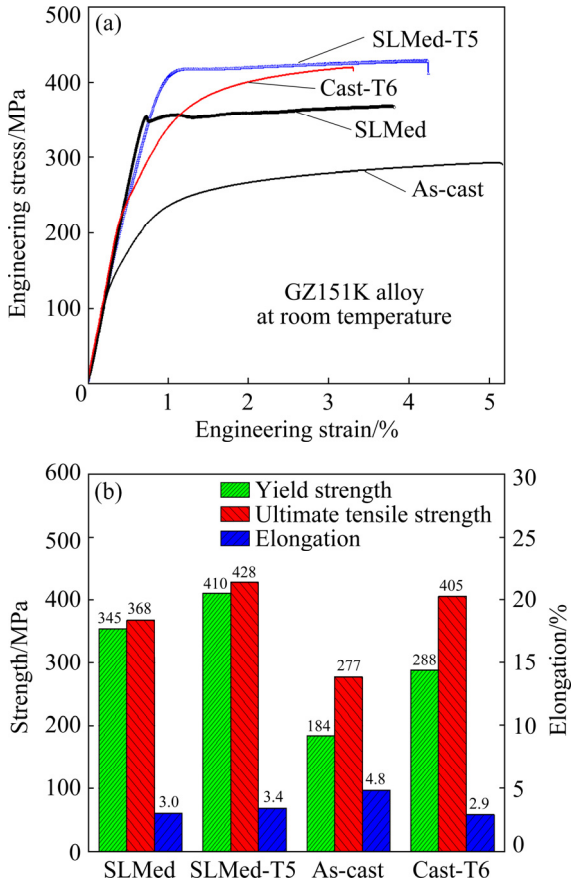

Fig. 7 Engineering stress−strain curves (a) and tensile properties (b) of SLMed and cast GZ151K alloys (data of cast GZ151K alloys come from Ref. [10])

The data of permanent mold cast GZ151K alloy [10] in as-cast and T6 conditions are also listed for comparison. From the stress−strain curves (Fig. 7(a)), it is obvious that the work hardening ability of the SLMed and SLMed-T5 alloys is much weaker than that of the as-cast and cast-T6 alloys. Yield strength (YS), ultimate tensile strength (UTS) and elongation of the SLMed GZ151K alloy are 345 MPa, 368 MPa and 3.0%, respectively. Compared with the as-cast alloy, the SLMed GZ151K alloy has obviously higher YS (increased by 161 MPa) and UTS (increased by 91 MPa), lower elongation (decreased by 1.8%). After T5 treatment, the YS of the SLMed-T5 GZ151K alloy increases to 410 MPa (increased by 65 MPa), the UTS increases to 428 MPa (increased by 60 MPa), while the elongation also increases to 3.4% (increased by 0.4%). Compared with the cast-T6 alloy, the SLMed-T5 GZ151K alloy has an obviously higher YS (increased by 122 MPa), a little bit higher UTS (increased by 23 MPa) and elongation (increased by 0.5%). Generally, the SLMed-T5 alloy has better mechanical properties than the cast-T6 alloy, specially the much higher YS, which is also clearly shown in the stress−strain curves in Fig. 7(a). The SLMed-T5 GZ151K alloy even has higher YS (increased by 30 MPa) and elongation (increased by 0.7%) than the extruded-T5 GZ151K alloy [32] (YS of 380 MPa, UTS of 461 MPa and elongation of 2.7%), with a lower UTS (decreased by 33 MPa).

Figure 8 shows the fracture surface morphologies of the SLMed, SLMed-T5, as-cast and cast-T6 GZ151K alloys. Compared with the cast alloys (Figs. 8(c, d)), the SLMed and SLMed-T5 alloys (Figs. 8(a, b)) have much finer fracture morphology, indicated by much finer fractured secondary phases (indicated by the arrows in Figs. 8(a, b)). These secondary phases are white and can be clearly distinguished in back-scattered electron SEM images. By contrast, the cast GZ151K alloys have much coarser secondary

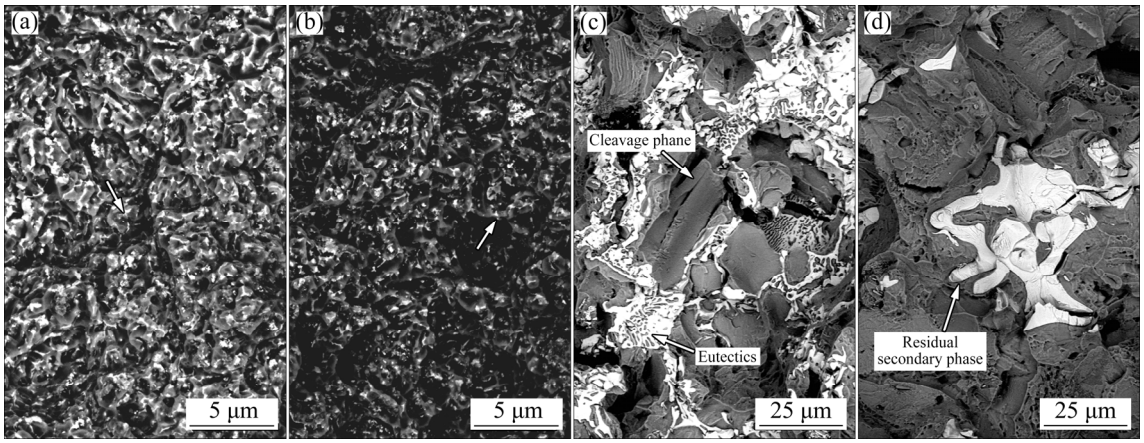

Fig. 8 Back-scattered electron SEM images of fracture surfaces of SLMed (a), SLM-T5 (b), permanent mold as-cast (c) and cast-T6 (d) GZ151K alloys

phases. In as-cast alloy, the network-shaped secondary phases are observed on the fracture surfaces, while in cast-T6 alloy, large solid residual secondary phases are visible. The cleavage planes are clearly observed in cast alloys (Figs. 8(c, d)), which are hard to be distinguished in the SLMed and SLMed-T5 alloys. The morphology differences of the fracture surfaces between the SLMed (Figs. 8(a, b)) and cast (Figs. 8(c, d)) GZ151K alloys come from their different microstructures. Much finer microstructure in the SLMed and SLMed-T5 GZ151K alloy leads to much finer fracture morphology.

4 Discussion

From the above results, it can be found that the microstructure of the SLMed GZ151K alloy is quite different from that of the conventional cast alloy. Compared with the cast alloy (Fig. 3(c), with average grain size of 41 μm [10]), the SLMed GZ151K alloy (Fig. 5) has much finer grains (~2 μm) and much finer secondary phases (Fig. 8(a)). Similar microstructure consisting of extremely fine grains was also reported in the SLMed WE43 Mg−RE alloys [22]. The refined microstructure should be mainly due to the high cooling rate of SLM process. The cooling rates of SLM process were reported in an order of 10^6 K/s [24]. Under such high cooling rate, AZ91D Mg alloy, which usually has larger grains (119 μm) under permanent mold casting [25], can even have grains as fine as 1.0−2.9 μm in SLM process [17]. It was reported that laser melting deposited (LMD) Mg−10Gd−3Y−Zr (wt.%, GW103K) Mg−RE alloy has an average grain size of ~19 μm [26], which is obviously higher than that of the SLMed GZ151K alloy (~2 μm) in the present study. Since GW103K and GZ151K Mg−RE alloys both contain lots of RE elements and their grains are both refined by Zr, it could be supposed that the cooling rate of the SLM process is much higher than that of the LMD process, though both of which are additive manufacturing processes for metals.

Besides the extra fine equiaxed-grains and secondary phases, weak textures and isotropic microstructures (Fig. 5) are also the characteristics of the SLMed GZ151K Mg−RE alloy, which are quite different from those of Fe [33], Ni [34] and Al [35] alloys fabricated by SLM process. Those alloys have columnar grains or dendrites growing towards the building direction.

Different from the general rule of which T5 treatment usually leads to the increase of yield strength and the decrease of elongation, the T5 treatment here increases both the yield strength and the elongation in the SLMed GZ151K alloy. Such behavior is probably related to the high cooling rate of the SLM process, which would generate high residual stress in the SLMed GZ151K alloy. The high residual stress corresponds well with the layer cracks (Fig. 1(b)), which are frequently observed even under the present optimized process parameters. The yield strength (345 MPa) of the SLMed GZ151K alloy is even higher than that of the extruded GZ151K alloy [32] (YS of 297 MPa, UTS of 368 MPa and elongation of 16.8%) under differential-thermal extrusion with similar average grain size of 2.5 μm. During the extrusion process, the billet and mold were preheated at ~490 and ~370 °C [32], respectively. Due to the heat exposure, the extruded GZ151K alloy is expected to have very low residual stress. Therefore, compared with the extruded alloy, the higher yield strength of the SLMed GZ151K alloy must be contributed to the high residual stress generated under high cooling rate. Hence, the SLMed GZ151K alloy is mainly strengthened by fine grains, fine secondary phases and residual stress during the SLM process. Compared with the SLMed alloy, after the subsequent aging at 200 °C, the YS and the elongation of the SLMed-T5 GZ15K alloy are increased by 65 MPa and 0.4%, respectively. Since the subsequent aging leads to the precipitation hardening (Figs. 6(b, c)) and probably releases part of the residual stress, it seems to be reasonable that the precipitation hardening improves the YS, while the release of the residual stress enhances the ductility. By contrary, the T5 treatment in extruded GZ151K alloy [32] leads to 83 MPa increment of YS (from 297 to 380 MPa), but 16.2% decrement of elongation (from 18.9% to 2.7%). Therefore, the abnormal phenomena that the T5 treatment increases both the yield strength and elongation in the SLMed GZ151K alloy, should be due to the high residual stress caused by the high cooling rate

of the SLM process. With the help of the residual stress, fine grains (Fig. 5) and secondary phases (Fig. 6(a)), precipitates (Figs. 6(b, c)), the YS and elongation of the SLMed-T5 GZ151K alloy are even higher than those of the extruded-T5 GZ151K alloy [32] (YS of 380 MPa, UTS of 461 MPa and elongation of 2.7%), though the UTS is 33 MPa lower. Therefore, the high yield strength of the SLMed-T5 GZ151K alloy is mainly due to fine grains, fine secondary phases, residual stress and precipitates.

5 Conclusions

(1) During the SLM process of GZ151K alloy, serious spattering appeared, which was much more obvious than those observed in steel, Ti or Al alloys. Layer cracks perpendicular to the building direction were frequently observed, which makes the mechanical properties fluctuate greatly. Therefore, the relationship between the spattering and the fluctuated mechanical properties needs to be revealed in future.

(2) Very fine grains (~2 μm), fine secondary phases and weak texture were fabricated in GZ151K alloy by the SLM process.

(3) The as-fabricated (SLMed) GZ151K alloy has YS of 345 MPa, UTS of 368 MPa and elongation of 3.0% at room temperature. After subsequent aging at 200 °C for 64 h (T5 treatment), both the strength and elongation increase. The YS, UTS and elongation of the SLMed-T5 GZ151K alloy are 410 MPa, 428 MPa and 3.4%, respectively, which are higher than those of the conventional cast-T6 alloy (YS of 288 MPa, UTS of 405 MPa and elongation of 2.9% [10]), specially the YS (122 MPa increment).

(4) The high yield strength of the SLMed GZ151K alloy mainly comes from fine grains, fine secondary phases and residual stress, while after T5 treatment, the alloy is further strengthened by precipitates.

Acknowledgments

ZRapid Tech Co., Ltd., and Tangshan Weihao Magnesium Powder Co., Ltd., are thankful for their support in SLM machine and GZ151K powder, respectively. The authors are grateful for financial supports from the National Key Research and Development Program of China (Nos. 2016YFB0301000, 2016YFB0701204), and the National Natural Science Foundation of China (No. 51821001).

References

[1] NIE J F. Precipitation and hardening in magnesium alloys [J]. Metallurgical and Materials Transactions A, 2012, 43: 3891−3939.

[2] FU Peng-huai, PENG Li-ming, JIANG Hai-yan, DING Wen-jiang, ZHAI Chun-quan. Tensile properties of high strength cast Mg alloys at room temperature: A review [J]. China Foundry, 2014, 11: 277−286.

[3] PAN Fu-sheng, YANG Ming-bo, CHEN Xian-hua. A review on casting magnesium alloys: Modification of commercial alloys and development of new alloys [J]. Journal of Materials Science & Technology, 2016, 32: 1211−1221.

[4] FU Peng-huai, PENG Li-ming, JIANG Hai-yan, ZHANG Zhen-yan, ZHAI Chun-quan. Fracture behavior and mechanical properties of Mg−4Y−2Nd−1Gd−0.4Zr (wt.%) alloy at room temperature [J]. Materials Science and Engineering A, 2008, 486: 572−579.

[5] SU Zai-jun, LIU Chu-ming, WAN Ying-chun. Microstructures and mechanical properties of high performance Mg−4Y−2.4Nd−0.2Zn−0.4Zr alloy [J]. Materials & Design, 2013, 45: 466−472.

[6] HE S M, ZENG X Q, PENG L M, GAO X, NIE J F. Microstructure and strengthening mechanism of high strength Mg−10Gd−2Y−0.5Zr alloy [J]. Journal of Alloys and Compounds, 2007, 427: 316−323.

[7] LI Ji-lin, CHEN Rong-shi, KE Wei. Microstructure and mechanical properties of Mg−Gd−Y−Zr alloy cast by metal mold and lost foam cast [J]. Transactions of Nonferrous Metals Society of China, 2011, 21: 761−766.

[8] OZAKI T, KUROKI Y, HOSHIKAWA H, YAMADA K, HOMMA T, KAMADO S. Effect of Cu addition on mechanical properties of Mg−Gd−Zn−Zr casting alloy [J]. Journal of Japan Institute of Light Metals, 2012, 62: 272−277.

[9] DING Zhi-bing, ZHAO Yu-hong, LU Ruo-peng, YUAN Mei-ni, WANG Zhi-jun, LI Hui-jun, HOU Hua. Effect of Zn addition on microstructure and mechanical properties of cast Mg−Gd−Y−Zr alloys [J]. Transactions of Nonferrous Metals Society of China, 2019, 29: 722−734.

[10] RONG Wei, WU Yu-juan, ZHANG Yu, SUN Ming, CHEN Juan, PENG Li-ming, DING Wen-jiang. Characterization and strengthening effects of γ' precipitates in a high-strength casting Mg−15Gd−1Zn−0.4Zr (wt.%) alloy [J]. Materials Characterization, 2017, 126: 1−9.

[11] WANG Dan, FU Peng-huai, PENG Li-ming, WANG Ying-xin, DING Wen-jiang. Development of high strength sand cast Mg−Gd−Zn alloy by co-precipitation of the prismatic β' and β_1 phases [J]. Materials Characterization, 2019, 153: 157−168.

[12] YAMADA K, HOSHIKAWA H, MAKI S, OZAKI T,

KUROKI Y, KAMADO S, KOJIMA Y. Enhanced age-hardening and formation of plate precipitates in Mg−Gd−Ag alloys [J]. Scripta Materialia, 2009, 61: 636−639.

[13] WANG Qu-dong, CHEN Jie, ZHAO Zheng, HE Shang-ming. Microstructure and super high strength of cast Mg−8.5Gd− 2.3Y−1.8Ag−0.4Zr alloy [J]. Materials Science and Engineering A, 2010, 528: 323−328.

[14] ZHANG Yu, WU Yu-juan, PENG Li-ming, FU Peng-huai, HUANG Fei. Microstructure evolution and mechanical properties of an ultra-high strength casting Mg−15.6Gd−1.8Ag−0.4Zr alloy [J]. Journal of Alloys and Compounds, 2014, 615: 703−711.

[15] PANG Song, WU Guo-hua, LIU Wen-cai, ZHANG Liang, DING Wen-jiang. Influence of pouring temperature on solidification behavior, microstructure and mechanical properties of sand-cast Mg−10Gd−3Y−0.4Zr alloy [J]. Transactions of Nonferrous Metals Society of China, 2015, 25: 363−374.

[16] JIANG Long-kang, LIU Wen-cai, WU Gua-hua, DING Wen-jiang. Effect of chemical composition on the microstructure, tensile properties and fatigue behavior of sand-cast Mg−Gd−Y−Zr alloy [J]. Materials Science and Engineering A, 2014, 612: 293−301.

[17] WEI Kai-wen, GAO Ming, WANG Ze-min, ZENG Xiao-yan. Effect of energy input on formability, microstructure and mechanical properties of selective laser melted AZ91D magnesium alloy [J]. Materials Science and Engineering A, 2014, 611: 212−222.

[18] NIU Xiao-miao, SHEN Hong-yao, FU Jian-zhong. Microstructure and mechanical properties of selective laser melted Mg−9 wt%Al powder mixture [J]. Materials Letters, 2018, 211: 4−7.

[19] WEI Kai-wen, WANG Ze-min, ZENG Xiao-yan. Influence of element vaporization on formability, composition, microstructure, and mechanical performance of the selective laser melted Mg−Zn−Zr components [J]. Materials Letters, 2015, 156: 187−190.

[20] WEI Kai-wen, ZENG Xiao-yan, WANG Ze-min, DENG Jin-feng, LIU Meng-na, HUANG Gao, YUAN Xiao-chi. Selective laser melting of Mg−Zn binary alloys: Effects of Zn content on densification behavior, microstructure, and mechanical property [J]. Materials Science and Engineering A, 2019, 756: 226−236.

[21] GANGIREDDY S, GWALANI B, LIU K M, FAIERSON E J, MISHRA R S. Microstructure and mechanical behavior of an additive manufactured (AM) WE43-Mg alloy [J]. Additive Manufacturing, 2019, 26: 53−64.

[22] ZUMDICK N A, JAUER L, KERSTING L C, KUTZ T N, SCHLEIFENBAUM J H, ZANDER D. Additive manufactured WE43 magnesium: A comparative study of the microstructure and mechanical properties with those of powder extruded and as-cast WE43 [J]. Materials Characterization, 2019, 147: 384−397.

[23] BAR F, BERGER L, JAUER L, KURTULDU G, SCHAUBLIN R, SCHLEIFENBAUM J H, LOFFLER J F. Laser additive manufacturing of biodegradable magnesium alloy WE43: A detailed microstructure analysis [J]. Acta Biomaterialia, 2019, 98: 36−49.

[24] LI Ya-li, GU Dong-dong. Parametric analysis of thermal behavior during selective laser melting additive manufacturing of aluminum alloy powder [J]. Materials & Design, 2014, 63: 856−867.

[25] CACERES C H, DAVIDSON C J, GRIFFITHS J R, NEWTO C L. Effects of solidification rate and ageing on the microstructure and mechanical properties of AZ91 alloy [J]. Materials Science and Engineering A, 2002, 325: 344−355.

[26] LIAO Hai-guang, FU Peng-huai, PENG Li-ming, LI Jia, ZHANG Shu-quan, HU Guo-qi, DING Wen-jiang. Microstructure and mechanical properties of laser melting deposited GW103K Mg–RE alloy [J]. Materials Science and Engineering A, 2017, 687: 281−287.

[27] MATSUDA M, LI S, KAWAMURA Y, LKUHRA Y, NISHIDA M. Interaction between long period stacking order phase and deformation twin in rapidly solidified $Mg_{97}Zn_1Y_2$ alloy [J]. Materials Science and Engineering A, 2004, 386: 447−452.

[28] HAGIHARA K, KINOSHITA A, SUGINO Y, YAMASAKI M, KAWAMURA Y, YASUDA H Y, UMAKOSHI Y. Effect of long-period stacking ordered phase on mechanical properties of $Mg_{97}Zn_1Y_2$ extruded alloy [J]. Acta Materialia, 2010, 58: 6282−6293.

[29] ZHANG Zhen-yan, PENG Li-ming, ZENG Xiao-qin, FU Peng-huai. Characterization of phases in a Mg−6Gd−4Sm−0.4Zr (wt.%) alloy during solution treatment [J]. Materials Characterization, 2009, 60: 555−559.

[30] NIE J F, OH-ISHI K, GAO X, HONO K. Solute segregation and precipitation in a creep-resistant Mg−Gd−Zn alloy [J]. Acta Materialia, 2008, 56: 6061−6076.

[31] WANG Dan, FU Peng-huai, PENG Li-ming, WANG Ying-xin, DING Wen-jiang. Quench sensitivity characterization of a LPSO-phase containing Mg alloy [J]. Materials Science and Engineering A, 2019, 749: 291−300.

[32] RONG Wei, ZHANG Yu, WU Yu-juan, CHEN Yuan-li, TANG Tao, PENG Li-ming, LI Da-yong. Fabrication of high-strength Mg−Gd−Zn−Zr alloys via differential-thermal extrusion [J]. Materials Characterization, 2011, 131: 380−387.

[33] GU Dong-dong, CHEN Hong-yu. Selective laser melting of high strength and toughness stainless steel parts: The roles of laser hatch style and part placement strategy [J]. Materials Science and Engineering A, 2018, 725: 419−427.

[34] NI Mang, CHEN Chao, WANG Xiao-jun, WANG Peng-wei, LI Rui-di, ZHANG Xiao-yong, ZOU Ke-chao. Anisotropic tensile behavior of in situ precipitation strengthened Inconel 718 fabricated by additive manufacturing [J]. Materials Science and Engineering A, 2017, 701: 344−351.

[35] KIMURA T, NAKAMOTO T, OZAKI T, SUGITA K, MIZUNO M, ARAKI H. Microstructural formation and characterization mechanisms of selective laser melted Al−Si−Mg alloys with increasing magnesium content [J]. Materials Science and Engineering A, 2019, 754: 786−798.

激光选区熔化增材制造高强度 Mg−15Gd−1Zn−0.4Zr 合金的显微组织与力学性能

付彭怀[1,2]，王南清[1]，廖海光[1]，徐雯钰[1]，彭立明[1]，陈 娟[1]，胡国琦[3]，丁文江[1]

1. 上海交通大学 轻合金精密成型国家工程研究中心&金属基复合材料国家重点实验室，上海 200240；
2. 上海轻合金精密成型国家工程研究中心有限公司，上海 201615；
3. 宁波工程学院 材料与化工学院，宁波 315211

摘 要：为了验证激光选区熔化(SLM)成型技术制造高性能镁−稀土合金的可行性，研究 SLM 工艺对 Mg–15Gd–1Zn–0.4Zr (质量分数，%) (GZ151K)镁合金显微组织与力学性能的影响。结果表明，打印态(激光选区熔化态)GZ151K 镁合金晶粒(约为 2 μm)和第二相细小、织构较弱；室温下，打印态 GZ151K 镁合金的屈服强度为 345 MPa，抗拉强度为 368 MPa，伸长率为 3.0%。200 °C、64 h 时效处理(T5)后，合金的屈服强度增加至 410 MPa、抗拉强度增加至 428 MPa、伸长率增加至 3.4%，拉伸性能均高于传统的重力金属型铸造 GZ151K-T6 合金，其中，屈服强度增幅高达 122 MPa。打印态 GZ151K 镁合金的主要强化机制为细晶、细小第二相和残余应力强化；经 T5 处理后，析出相进一步提高合金的屈服强度。

关键词：激光选区熔化；镁−稀土合金；晶粒细化；Mg–Gd–Zn；强化机制

(Edited by Wei-ping CHEN)